An Error Area Determination Approach in Machining of Aero-engine Blade

ZHANG Yun[1], *ZHU Yu*[2*], *ZHU Zhengqing*[3]

1. School of Mechanical and Materials Engineering, North China University of Technology, Beijing 100144, P. R. China;
2. AVIC Manufacturing Technology Institute, Beijing 100024, P. R. China;
3. School of Mechanical Engineering and Automation, Beihang University, Beijing 100191, P. R. China

(Received 22 February 2021; revised 10 June 2021; accepted 29 October 2021)

Abstract: As a result of the recently increasing demands on high-performance aero-engine, the machining accuracy of blade profile is becoming more stringent. However, in the current profile, precision milling, grinding or near-net-shape technology has to undergo a tedious iterative error compensation. Thus, if the profile error area and boundary can be determined automatically and quickly, it will help to improve the efficiency of subsequent re-machining correction process. To this end, an error boundary intersection approach is presented aiming at the error area determination of complex profile, including the phase Ⅰ of cross sectional non-rigid registration based on the minimum error area and the phase Ⅱ of boundary identification based on triangular meshes intersection. Some practical cases are given to demonstrate the effectiveness and superiority of the proposed approach.

Key words: aero-engine blade; error area; boundary identification; non-rigid registration; NC re-machining

CLC number: TH164 **Document code:** A **Article ID:** 1005-1120(2022)03-0349-09

0 Introduction

Aero-engine blade possesses complex profile and strict design tolerance, which has always been regarded as the difficulty in aeronautical manufacturing. During the finishing process of blade profile before mass production, because of the effect of elastic and permanent deformation fractions, the iterative correction process of error compensation is always necessary but tedious[1]. The most common method used by technologists is to modify the NC program to obtain a more accuracy profile.

The main manufacturing errors of blade profile are from geometric and thermo-mechanical error of machine tool, deflection errors of cutting tool, workpiece and machine tool structure, dynamic errors of motion control method and software[2]. There are a lot of approaches to compensate these error sources[3-4], especially the machining-related[5], which is always compensated by online re-machining technology[6]. However, the necessary error area and boundary for blade profile are considered by manual operations with non-automation and poor-efficiency. The current digital determination focusses on the extraction and classification of scanning data geometric attributes. Two main principles are found in Refs.[7-10]: (1) Curvature method, (2) normal vector method. These researches are carried out for extreme points of principal curvature and abrupt points of normal vectors in the main direction of the scanned data. However, the curvature and normal vectors of the blade profile possess complex variation, especially in the case of small machining allowance, it is difficult to determinate the geometric attributes by the aforementioned principles. In order to achieve the numerical control and automation of the blade profile error compensation, the paper carries out a boundary intersection method.

*Corresponding author, E-mail address: zhuyork@sina.com.

How to cite this article: ZHANG Yun, ZHU Yu, ZHU Zhengqing. An error area determination approach in machining of aero-engine blade[J]. Transactions of Nanjing University of Aeronautics and Astronautics, 2022, 39(3): 349-357.

http://dx.doi.org/10.16356/j.1005-1120.2022.03.009

1 Overview and Terminology

In order to achieve high efficiency for re-machining technology[11], the proposed approach includes two phases: the phase Ⅰ of cross sectional non-rigid registration based on the minimum error area and the phase Ⅱ of boundary identification based on triangular meshes intersection, where the minimum area objective function is used to reduce the subsequent re-machining time. Because design tolerance constraints are introduced in solving the objective function, the profile deformation distribution is approximated by the transformation and rotation of several typical cross sections under the assumption of continuous distribution of blade profile deformation[12], reducing the computational complexity of solving constrained non-linear optimization problem. Subsequently, the triangle-triangle intersection is carried out between the measured data and the tolerance surface of the optimum blade profile. Then the closed and open loops of error boundaries are identified by the intersection point sorting algorithms. The flowchart of the proposed approach is shown in Fig.1.

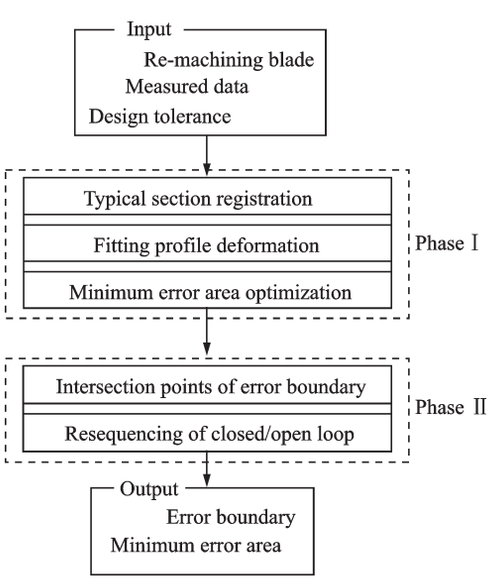

Fig.1 Flowchart of the proposed approach

The proposed approach follows the basic principle of blade design from simplicity to complexity, namely from cross sections to skinning profile. Fig.2 shows the cross-sectional form-position tolerance, which consists of displacement (ϕ), orientation (φ), and profile tolerance (υ_r or υ_s)[13-14]. Measured data can be rigidly transformed to the optimal position through translation and rotation matrixes in the Section 2.1, which is composed of two translations (T_x, T_y) and one rotation (R_z), and the relational inequalities are given by Eq.(1) for rigid transformation purpose.

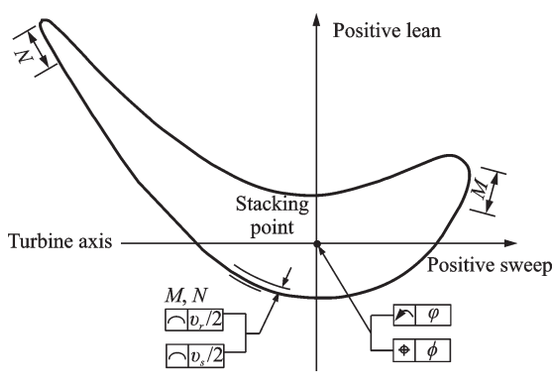

Fig.2 Cross-sectional sketch of aero-engine blade

$$\begin{cases} \max\left(R_z\right) \leqslant \varphi \\ \left(T_x\right)^2 + \left(T_y\right)^2 \leqslant \left(\dfrac{\phi}{2}\right)^2 - \dfrac{\upsilon_s}{2} \leqslant \upsilon \leqslant \dfrac{\upsilon_s}{2} \end{cases} \tag{1}$$

The measured data are conducted with two different devices, CMM CENTURY 977 (AVIC BPEI, Beijing, China; Renishaw TP7M touch trigger probe) and GOM ATOS Ⅱ-400 (GOM mbH, Braunschweig, Germany). Our previous research[15] is helpful to improve the accuracy and efficiency of measured data, and the slicing process is adopted on each cross section, as shown in Fig.3.

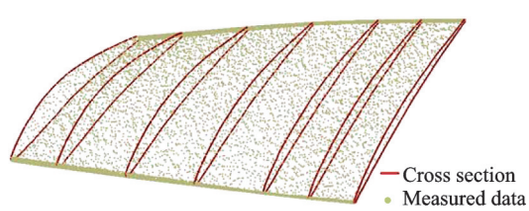

Fig.3 Measured data and slicing process

2 Algorithm and Implement

With the development of computer-aided design, there are some differences in the representation and properties of the blade profile. For conve-

nience in exposition, Fig.4 shows the nominal $E=\{E_i|i=0,\cdots,m-1\}$ cross-sectional curves can be written as[16] $U_i=\sum_{j=0}^{n-1}N_{j,3}(u)\cdot d_{i,j}$ with $u\in[0,1]$. In the v-direction its spline can be written as $V_j'=\sum_{i=0}^{m'}N_{i,3}(v)\cdot\phi_{i,j}(j=0,\cdots,n-1)$ with $v\in[0,1]$, where $\{\phi_{0,j},\cdots,\phi_{m',j}\}$ are control points of the cubic B-splint curve with data points $\{d_{0,j},\cdots,d_{m-1,j}\}$. Thus, the blade profile can be expressed as

$$W=\sum_{i=0}^{m'}\sum_{j=0}^{n-1}N_{i,3}(u)\cdot N_{j,3}(v)\cdot\phi_{i,j} \tag{2}$$

where $N_{i,3}(u)$, $N_{j,3}(v)$ are the normalized B-spline basis function of degree 3.

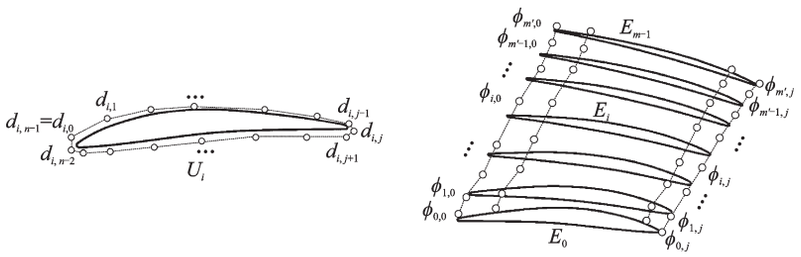

Fig.4 Sketch of blade profile representation

2.1 Phase Ⅰ

Step 1 Select r ($3\leqslant r\leqslant m$) cross sections form E and build subset $S=\{S_{i'}|i'=0,\cdots,r-1\}\subseteq E$, their cross-sectional curves $C=\{C_{i'}|i'=0,\cdots,r-1\}\subseteq U=\{U_i|i=1,\cdots,m-1\}$ is the $v'=\{v_{i'}'|i'=0,\cdots,r-1\}\subseteq v=\{v_i|i=1,\cdots,m-1\}$ constant iso-parameter curve of W.

The cross sectional non-rigid registration between $C_{i'}$ and M measured points. The basic idea is similar to the classical iterative closest point (ICP) algorithm[17]. It is also iterative in nature, which means that the algorithm developed can be formulated as an objective function by the least squares principle of rigid registration, and produces a sequence of non-rigid transformation matrixes $\boldsymbol{H}_{i'}(T_{xi'},T_{yi'},R_{zi'})$ as follows

$$\min f=\sum(P_{i'}-\boldsymbol{H}_{i'}\cdot Q_{i'})^2$$
$$\text{s.t. } R_{zi'}\leqslant\varphi\cap\left[(T_{xi'})^2+(T_{yi'})^2\right]\leqslant\left(\frac{\phi}{2}\right)^2 \tag{3}$$

where $P_{i'}$ is the closest point in $C_{i'}$ corresponding to $Q_{i'}$. It should be noted that the subset $Q_{i'}$ has few or all elements equal to the measured points on the cross section $S_{i'}$ and satisfies Euclidean distance $|P_{i'}Q_{i'}|\leqslant\upsilon_s/2$ in each iteration, as shown in Fig.5. In other words, if the Euclidean distance from the measuring point to $C_{i'}$ is more than $\upsilon_s/2$, the measured point will not be brought into Eq.(3).

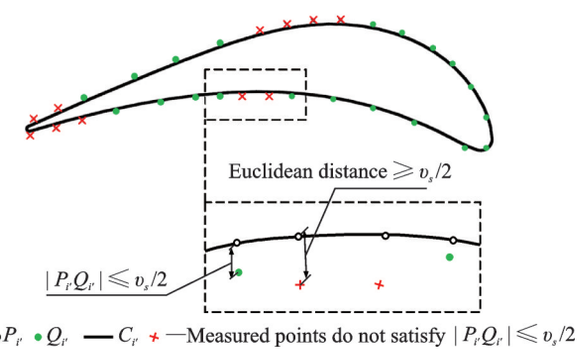

Fig.5 Sketch of non-rigid registration for $P_{i'}$ and $Q_{i'}$

Step 2 Polynomial fitting with v variable on $v'=\{v_{i'}'|i'=0,\cdots,r-1\}$ and $\boldsymbol{H}=\{\boldsymbol{H}_{i'}|i'=0,\cdots,r-1\}$ is

$$f_H(v)=\sum_{t=0}^{r-1}b_tv^t$$
$$\text{s.t. } f_H(v_{i'}')=\boldsymbol{H}_{i'}\quad i'=0,\cdots,r-1 \tag{4}$$

As shown in Fig.6, the non-rigid registration matrix $f_H(v_i)(i=0,\cdots,m-1)$ can be obtained by interpolation for $U=\{U_i|i=1,\cdots,m-1\}$, i. e. $U_i'=f_H(v_i)\cdot U_i$ and its control point $d_{i,j}'=f_H(v_i)\cdot d_{i,j}$.

Step 3 Construct cubic B-spline $V_j'=\sum_{i=0}^{m'}N_{i,3}(v)\cdot\phi_{i,j}'(j=0,\cdots,n-1)$ with data points $\{d_{0,j}',\cdots,d_{m-1,j}'\}$ in the v-direction. Thus, the blade profile after non-rigid registration can be expressed as

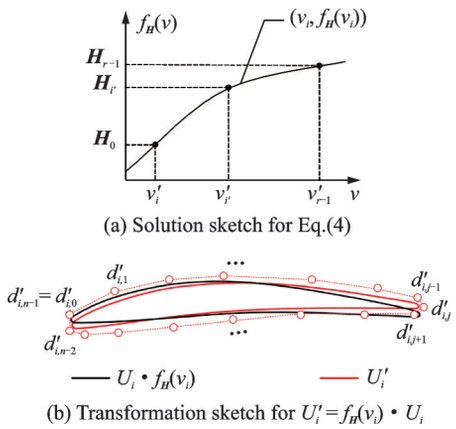

Fig.6 Sketch of Step 2 for $U_i'=f_H(v_i)\cdot U_i$

$$W'(u,v)=\sum_{k=0}^{m'}\sum_{j=0}^{n-1}N_{k,3}(u)N_{l,3}(v)\phi'_{k,l} \tag{5}$$

Due to the difficulty in achieving a sequence of fitting coefficients $B=\{b_0,\cdots,b_t,\cdots,b_r\}$ of Eq.(4) within the limited time period of optimization, an efficient approximation operation is developed to identify triangular patches of measured points that are above the upper tolerance $(v_s/2)$ boundary surface of $W'(u,v)$. The area sum of these possible error patches is considered as error area. Fig.7 shows the minimum directional distance d_g between $W'(u,v)$ and the center point c_g of triangular patches T_g, $g=1,2,\cdots,M\in N^*$. A_g is the patch area of T_g. It is also iterative in nature, which means that the error-area determination can be formulated as an objective function by the minimal area principle of registration fitting and generates $B=\{b_0,\cdots,b_t,\cdots,b_r\}$, as Eq.(6). The iterative process (Steps 1—3) may be continued until the objective function difference $\Delta\min F(D)$ between every two iterations is equal or less than specified thresholds, then the optimum blade profile $W'(u,v)$ after non-rigid registration can be constructed, denoted by $W''(u,v)$.

$$\begin{cases}\min F(D)=\sum\lambda_g\cdot A_g\\ \lambda_g=\begin{cases}0 & -\dfrac{v_s}{2}<h_g<\dfrac{v_s}{2}\\ 1 & h_g>\dfrac{v_s}{2}\cup h_g<-\dfrac{v_s}{2}\end{cases}\\ g=0,1,2,\cdots\end{cases} \tag{6}$$

It is assumed that the number of measured points is N on each cross section, then the time complexity of Eq.(3) is $O(rN)$. In the course of solving $\min F(D)$, the minimum distance calculation is required for M measuring points, then the time complexity of Eq.(6) is $O(M+rN)$.

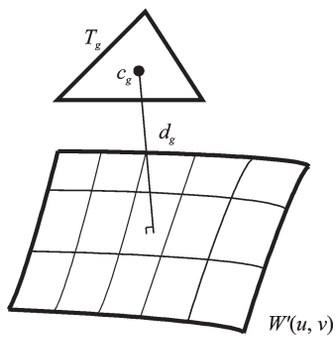

Fig.7 The minimum directional distance d_g between center point c_g of triangular patches T_g and $W'(u,v)$

2.2 Phase Ⅱ

After the approximation-based non-rigid registration, $W''(u,v)$ can meet the requirements of position tolerance (ϕ,φ) and the minimum error area, then the error boundary can be identified through computer graphic intersection algorithms[18]. Specifically, the error area can be defined as outer points of the upper tolerance $(v_s/2)$ surface of $W''(u,v)$, which can be obtained by the surface offset algorithm. Considering the triangulation convenience of M measuring points and the tolerance boundary surface, the error boundary is obtained by triangle-triangle intersection algorithms. Fig.8 shows the result of intersection points.

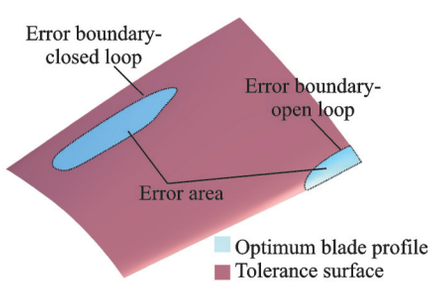

Fig.8 Results of error boundary identification

There are two types of the error boundary: (1) Closed loops that represent these intersection points are away from the profile edges, and (2) open loops that represent endpoints reach to the profile edges. Fig.9 shows the initial sequence of intersection points. The sequence can be changed based on the distance threshold for each neighboring point, then

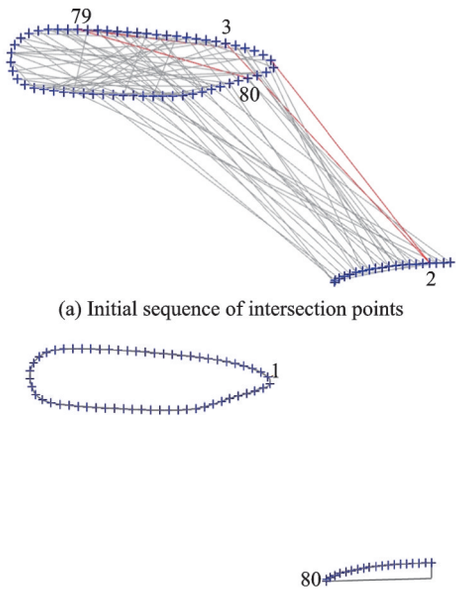

(a) Initial sequence of intersection points

(b) Error boundary: One open loop and one closed loop

Fig.9 Closed/open loops and error area

the final sequence of intersection points is linked to form the error boundary. There is one open loop and one closed loop, inside which are identified as error area.

3 Results and Discussion

In order to illustrate the validity and advancement of the proposed approach, three practical cases are presented.

3.1 Precision forging blade

One practical case is a precision forging blade with the size of 60 mm × 90 mm, in which ϕ = 0.1 mm, υ_s = 0.08 mm ([−0.03 mm, +0.05 mm]), and $\varphi = \pm 8'$, as shown in Fig.10(a). It is known that the machining region is the neighboring areas of leading/trailing edge (LE/TE) due to the precision forging process. Fig.10(b) shows the measured data acquired by the 3D-optical scanning system (GOM ATOS Ⅱ-400), and its error distribution illustrates that the initial machining region is pressure/suction side (PS/SS). By reference to the phase Ⅰ, three typical cross sections (i.e., sections ①/②/③) are conducted non-rigid registration to realize the localization of cross-sectional curves.

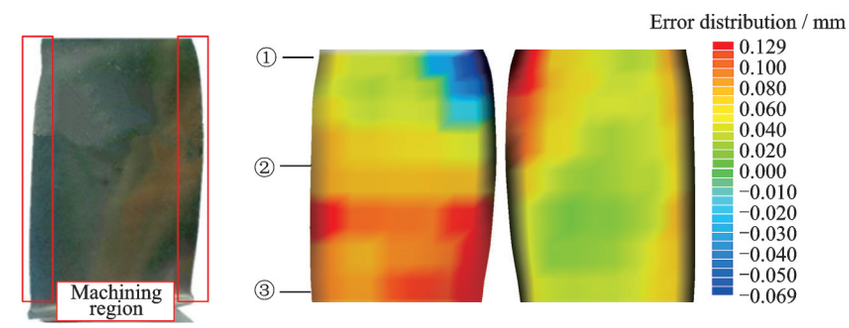

(a) Precision forging blade (b) Measured data and error distribution

Fig.10 Precision forging blade and measured data and error distribution

The situation that $Q_{i'}$ has few or all elements equal to the measured data and does not satisfy υ_s = 0.08 mm (defined in red) is not considered during the initial iterations. Figs.11(a—c) show the variation of error curves(Error(mm)) of the sections ①/②/③ with the increase of corresponding points ($\{P_{i'}, Q_{i'}\}$, defined in yellow) after each iteration (Iteration num(No.)). A sequence of transformations and rotations are listed in Table 1.

Fig.12 illustrates the error distribution between the optimum blade profile and measured data after phase Ⅰ. Furthermore, the error boundary (black lines) are two open loops after phase Ⅱ, which basical-

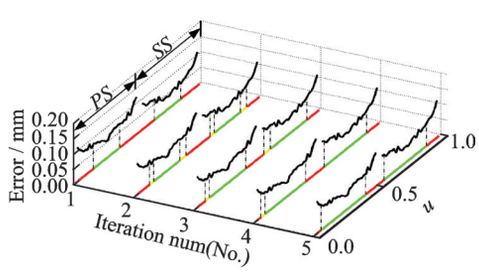

(a) Section ①

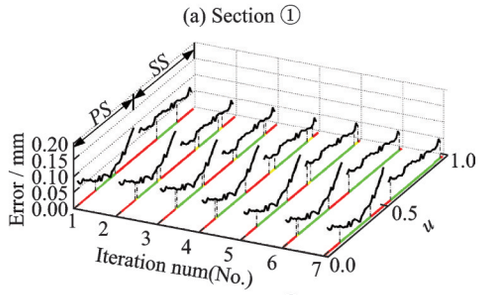

(b) Section ②

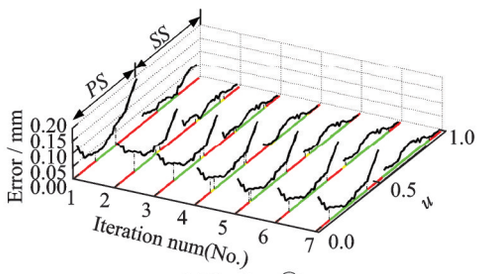

(c) Section ③

— Q_i has few or all elements equal to the measured data and satisfies $|v_s| \geqslant$[−0.03 mm, +0.05 mm]

— Q_i has few or all elements equal to the measured data and has not satisfy $|v_s| \geqslant$[−0.03 mm, +0.05 mm]

— The new adding corresponding points for each iteration

Fig.11 Variation of error curves after each iteration of non-rigid registration

Table 1 Non-rigid registration of three typical cross sections

Section	Rotation/(′)	Translation/mm
①	−2.34	(−0.041 8, +0.003 2)
②	−0.16	(−0.023 5, −0.018 4)
③	+7.27	(+0.038 0, −0.042 4)

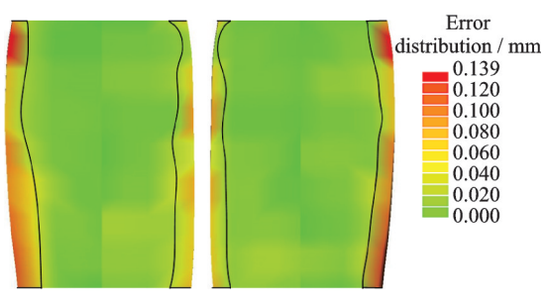

Fig.12 Error distribution and boundary identification for precision forging blade

ly tallies with the result by an experiential judgement.

3.2 High-precision grinding blade

Another practical case is a high-pressure compressor blade with complex profile, in which $\varphi = 12'$, $\phi = 0.1$ mm, $v_s = 0.06$ mm ([−0.02 mm, +0.04 mm]). There are still unstable grinding error areas due to its difficult-to-machine materials and thin-wall structure[19]. Therefore, it is an essential step for error compensation to carry out the boundary identification on the experiment process. The GOM ATOS Ⅱ-400 is utilized to acquire measured data, as shown in Fig.13. We use five typical cross sections (i.e., sections ①—⑤) to conduct non-rigid registration and generate a sequence of transformations and rotations in Table 2.

After the phase Ⅰ, Fig.14 shows the error distribution between the measured data and the optimum blade profile. The error area shares about 5.5% of the total profile area. Thus, the error boundaries are identified through the triangle-triangle intersection algorithm, including one closed loop and two open loops as shown in Fig.15.

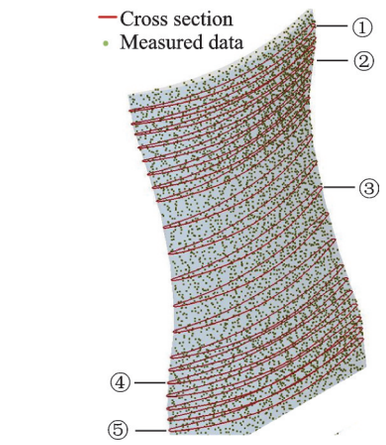

Fig.13 Tested blade and five typical cross sections

Table 2 Non-rigid registration of five typical cross sections

Section	Rotation/(′)	Translation/mm
①	+0.294	(−0.016 6, 0.005 1)
②	+1.566	(−0.022 6, −0.002 0)
③	+3.734	(−0.015 0, 0.001 9)
④	−1.302	(0.020 2, −0.002 5)
⑤	−5.454	(0.022 8, −0.000 2)

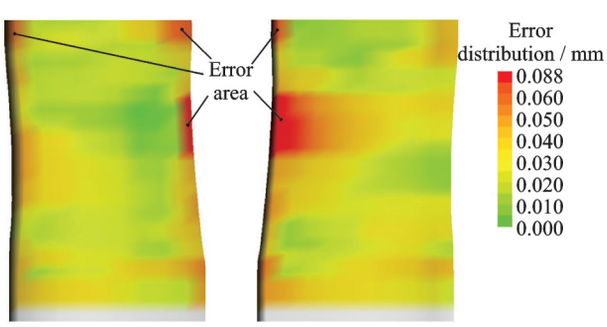

Fig.14 Error distribution displayed by color cloud

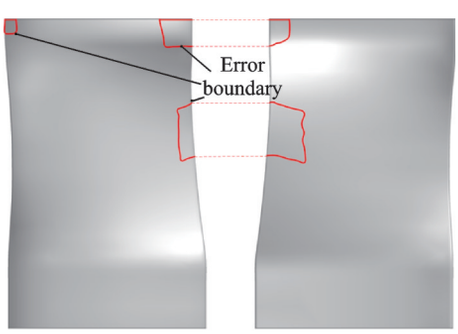

Fig.15 Error boundary

Through modifying the cutter path based on the boundary information, the error area can be compensated automatically. Fig.16 shows the error distribution can satisfy the design requirements.

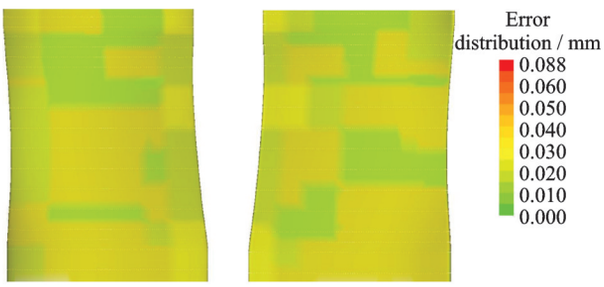

Fig.16 Error distribution after error compensation

3.3 Investment casting turbine blade

The other practical case is an investment casting turbine blade (Fig.17(a)), in which $\upsilon_s = 0.14$ mm ([−0.07 mm, +0.07 mm]). GOM ATOS Ⅱ-400 is utilized to acquire measured data, as shown in Fig.17(b). According to the previous engineering experience, the error area is distributed in the pressure side, and the error boundary is closed loop. Because the curvature and normal vector change is not obvious in this case of small machining allowance, the geometric attribute identification method mentioned in the introduction is not suitable for determining the error area. Thus, Fig.17(c) illustrates the error distribution between the optimum blade profile and measured data after phase Ⅰ, and four closed loops of the error boundary are identified, as shown in Fig.17(d).

(a) Investment casting turbine blade

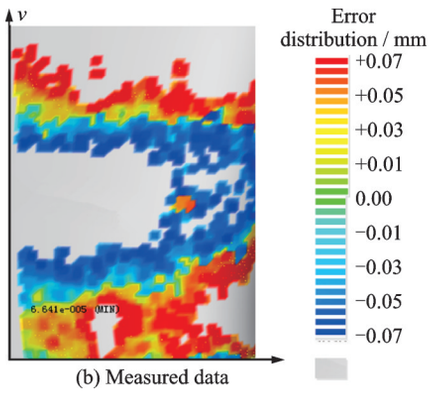

(b) Measured data

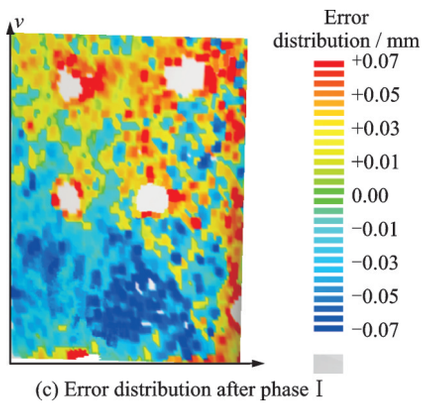

(c) Error distribution after phase Ⅰ

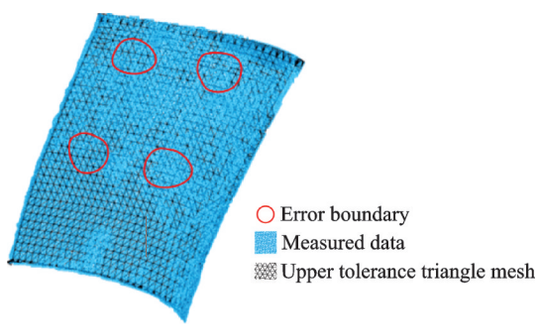

(d) Error boundary (four closed loops)

Fig.17 Resluts of investment casting turbine blade

4 Conclusions

Due to the inevitable deformation of the aero-engine blade with the difficult-to-machining materials and complex profile, the high precision blade needs to undergo a tedious iterative correction process of error compensation. It is crucial for process engineers to determinate the profile error area and boundary automatically and quickly. To this end, we have proposed an error area determination approach, which consists of two phases: The non-rigid registration based on the minimum error area and the boundary identification based on triangular meshes intersection. The decoupled solution ensures the

efficiency and superiority of the developed algorithms to preserve an optimum compromise by minimizing error areas and conforming design tolerance at most degree for the implementation of subsequent re-machining.

Under the framework of the proposed approach, emphasis of further research activities will be conducted in solving the unfairness problem of the error boundary, which will help to a speed-generating re-machining tool path and bring more automation and intelligence to error compensation.

References

[1] LASEMI A, XUE D, GU P. A freeform surface manufacturing approach by integration of inspection and tool path generation[J]. International Journal of Production Research, 2012, 50(23): 6709-6725.

[2] MEHRAD V, XUE D, GU P. Inspection of freeform surfaces considering uncertainties in measurement, localization and surface reconstruction[J]. Measurement Science and Technology, 2013. DOI: 10.1088/0957-0233/24/8/085008.

[3] LIU C, LI Y, SHEN W. A real time machining error compensation method based on dynamic features for cutting force induced elastic deformation in flank milling[J]. Machining Science and Technology, 2018, 22(4/5/6): 766-786.

[4] BLASER P, PAVLIČEK F, MORI K, et al. Adaptive learning control for thermal error compensation of 5-axis machine tools[J]. Journal of Manufacturing Systems, 2017, 44: 302-309.

[5] CHEN X Z, ZHU D, XU Z, et al. Dissolution characteristics of new titanium alloys in electrochemical machining[J]. Transactions of Nanjing University of Aeronautics and Astronautics, 2016,33(5): 610-619.

[6] LIU H B, WANG Y Q, JIA Z Y, et al. Integration strategy of on-machine measurement (OMM) and numerical control (NC) machining for the large thin-walled parts with surface correlative constraint[J]. The International Journal of Advanced Manufacturing Technology, 2015, 80(9/10/11/12): 1721-1731.

[7] MILROY M J, BRADLEY C, VICKERS G W. Segmentation of a wrap-around model using an active contour[J]. Computer Aided Design, 1997, 29(4): 299-320.

[8] ISMAIL E. Feature extraction of laser scan data based on geometric properties[J]. Journal of the Indian Society of Remote Sensing, 2016, 45(1): 1-10.

[9] ANGELO L D, STEFANO P D. Geometric segmentation of 3D scanned surfaces[J]. Computer-Aided Design, 2015, 62: 44-56.

[10] WOO H, KANG E, WANG S, et al. A new segmentation method for point cloud data[J]. International Journal of Machine Tools & Manufacture, 2002, 42(2): 167-178.

[11] HUANG N, BI Q, WANG Y, et al. 5-axis adaptive flank milling of flexible thin-walled parts based on the on-machine measurement[J]. International Journal of Machine Tools and Manufacture, 2014, 84: 1-8.

[12] HSU T H, LAI J Y, UENG W D. On the development of airfoil section inspection and analysis technique[J]. International Journal of Advanced Manufacturing Technology, 2006, 30(1/2): 129-140.

[13] ZHANG Y, CHEN Z T, NING T. Reverse modeling strategy of aero-engine blade based on design intent[J]. The International Journal of Advanced Manufacturing Technology, 2015, 81(9/10/11/12): 1781-1796.

[14] WANG Jie, ZHAO Miaodong, MAO Jianxing. Parametric modeling system for cooling turbine blade based on feature design[J]. Transactions of Nanjing University of Aeronautics and Astronautics, 2020, 37(5): 758-767.

[15] ZHANG Y, CHEN Z T, NING T. Efficient measurement of aero-engine blade considering uncertainties in adaptive machining[J]. International Journal of Advanced Manufacturing Technology, 2016, 86(1): 1-10.

[16] PIEGL L A, TILLER W. The NURBS book[M]. New York: Springer, 1997: 35-38.

[17] BESL P J, MCKAY H D. A method for registration of 3-D shapes[J]. IEEE Transactions on Pattern Analysis & Machine Intelligence, 1992, 14(2): 239-256.

[18] PCL. Point cloud library [DB/OL]. (2021-05-21). http://www.pointclouds.org/documentation/.

[19] MENG F J, LI X, CHE Z T, et al. Study on the cantilever grinding process of aero-engine blade[J]. Proceedings of the Institution of Mechanical Engineers, Part B: Journal of Engineering Manufacture, 2014, 228(11): 1393-1400.

Acknowledgement This work was supported by the Aeronautical Science Foundation of China (No.

20200016112001).

Authors Dr. **ZHANG Yun** received the Ph.D. degree in mechanical engineering from Beihang University, Beijing, China, in 2016. From 2020 to present, he has been with School of Mechanical and Materials Engineering, North China University of Technology. His research has focused on complex surface CAD/CAM software, adaptive machining technology of blade and blisk for an aerospace engine.

Dr. **ZHU Yu** received the Ph.D. degree in mechanical engineering from Beihang University, Beijing, China, in 2017. Then he joined in AVIC Manufacturing Technology Institute in August 2017, where he is a senior engineer. His research is focused on CAD/CAM software, polishing system, and machining technology of blade and blisk for an aerospace engine.

Author contributions Dr. **ZHANG Yun** proposed the idea, implemented the research process and revised the manuscript. Dr. **ZHU Yu** provided instructional support, designed research plans and interpreted the results. Dr. **ZHU Zhengqing** conducted the analysis and wrote the manuscript. All authors commented on the manuscript draft and approved the submission.

Competing interests The authors declare no competing interests.

(Production Editor: XU Chengting)

航空发动机叶片数控加工区域误差识别方法

张 云[1], 朱 燏[2], 朱正清[3]

(1.北方工业大学机械与材料工程学院, 北京 100144, 中国; 2.中国航空制造技术研究院, 北京 100024, 中国; 3.北京航空航天大学机械工程及自动化学院, 北京 100191, 中国)

摘要: 随着对航空发动机性能要求的不断提高,叶片型面加工精度要求愈加严格。然而,目前常用的型面精加工方式中,精密铣削、磨削或近净成形工艺在工艺定形前都需要经过烦琐的迭代误差补偿。而在该过程中若能快速确定误差区域和边界将有助于提高后续迭代过程的效率。为此,本文提出了一种针对叶片复杂型面误差区域自动识别的最小面积误差区域边界求交方法,包括基于最小误差区域的截面非刚性配准和基于三角网格求交的边界识别。应用实例说明了该方法的有效性和优越性。

关键词: 航空发动机叶片;误差区域;边界识别;非刚性配准;数控补加工